Chapter

Strongly Fluorescent Heterocyclic Molecule: Crystallography, 3D Hydrogen-Bonded, Fluorescence Study and QTAIM/TD-DFT/MESP Theoretical Analysis

Ouahida Zeghouan, Seifeddine Sellami and Mohamed AbdEsselem Dems

Abstract

In this chapter we explored the fluorescence properties of the title compound 1–10 phenanthroline hydrate (phh), $\{(C_{12}N_2H_8)\cdot H_2O\}$. The structure of phh is stabilized by strong as well as weak intermolecular interactions in the crystal. These interactions O—H⋯O, O—H⋯N, C—H⋯O and C—H⋯N hold the crystal structure in a three-dimensional network. Optical analysis (fluorescence) was performed on the test compound. The measurements in solvents of different polarities were carried out at ambient temperature (298 K). These results prompted us to investigate some photoluminescence applications for heterocyclic compounds as the sensing of blue-light luminescent materials. The time-dependent density functional theory (TD-DFT) calculations were performed on this compound, with the purpose to identify the origin of absorption and emission band, the nature of the electronic transitions. The atoms in molecules (AIM) theory and orbital analysis and molecular electrostatic potential (MESP) were applied to analyze the electron densities, their properties and the energy diagram of the molecular orbitals. The AIM and MESP analysis have been applied for part B of phh to demonstrate that the O1W—H11W⋯N1B type of interaction has the strongest hydrogen bond.

Keywords: aromatic molecule, X-ray diffraction, fluorescence, QTAIM/TD-DFT/MESP theoretical analysis

1. Introduction

The study of the photochemical and photophysical properties of heterocyclic compounds has received a great deal of attention during the last decade. 1,10-phenanthroline hydrate is a heterocyclic organic compound, used as a ligand in coordination chemistry; it has been the object of numerous studies, owing to its excellent complexing properties on metal ions. The multitude of applications of this cation motivated large development in synthesis of phenanthroline [1]. Various physico-chemical and biochemical techniques including UV/visible, fluorescence

and viscometric titration, thermal denaturation and differential pulse voltammetry have been employed for 1,10-phenanthroline complexes to probe the details of DNA binding [2, 3]. The influence of the presence of nitrogen atoms on the fluorescence spectral maxima of aromatic molecules is our interest, including comparison of the spectra in polar and non-polar solvents. Such studies facilitate to understand the features of chemical bonding in molecules from the topological analysis of electron densities [4] and various electrostatic properties of molecules. These fundamental properties are directly related to the properties of materials [5]. The present compound, viz. $\{(C_{12}N_2H_8)\cdot H_2O\}$, has been characterized with X-ray crystallography, and we are interested in fluorescence properties. The fluorescence spectra of the present compound have been obtained in various conditions. The time-dependent density functional theory (TD-DFT)/quantum theory of atoms in molecules (QTAIM)/orbital analysis and molecular electrostatic potential (MESP) theoretical calculations have been applied too.

2. Structural commentary

The structure of $\{(C_{12}N_2H_8)\cdot H_2O\}$ is trigonal; space group P31, the molecular structure, is shown in **Figure 1**. The asymmetric unit is formed from three molecules of phenanthroline and three molecules of water. The crystal structure is built of successive rings formed by six molecules of phenanthroline; the centre of these
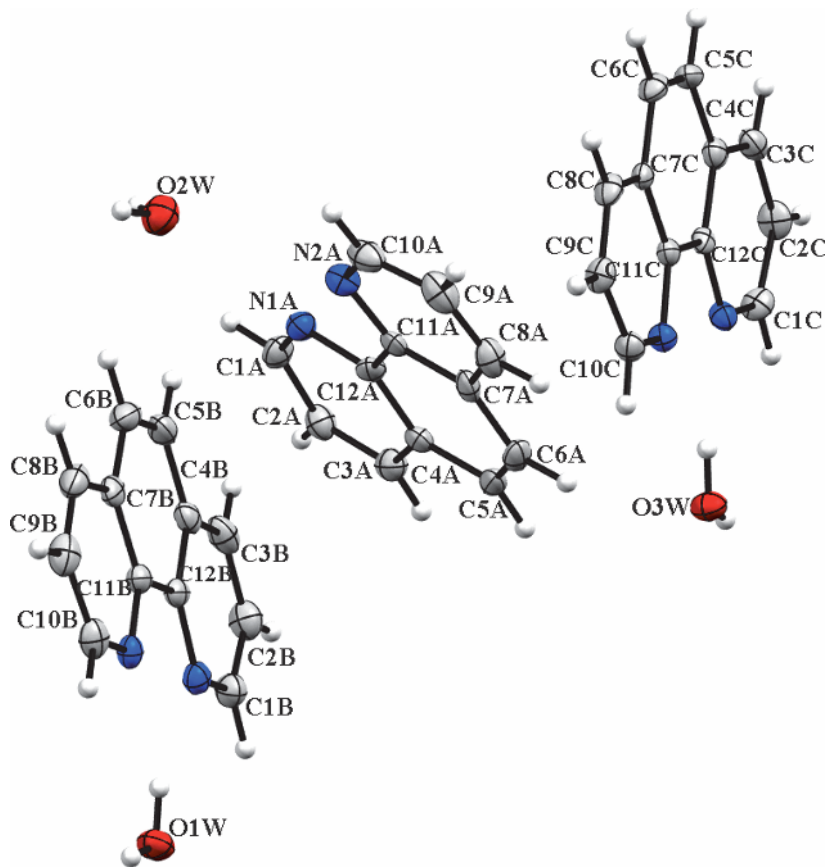

Figure 1.
View of the hpp molecule, with the atom-numbering scheme. Displacement ellipsoids are drawn at the 50% probability level, and H atoms are shown as circles of arbitrary radii.

rings are the three molecules of water. Bond lengths and valence angles compare well with the average values from related phenanthroline structures [6, 7].

3. Supramolecular features

The crystal structure is built of successive rings of phenanthroline and water molecules extending parallel to (001) plane that are connected by an extensive three-dimensional hydrogen-bonded network of the type O—H⋯O, O—H⋯N, C—H⋯O and C—H⋯N (**Table 1** and **Figure 2a**). Aqua molecules and N groups are involved in hydrogen bonding and form a three-dimensional network of infinite chains and variable degrees of rings [$C^3_3(7)$, $R^2_1(5)$, $R^2_2(9)$, $R^5_6(22)$ and $R^4_6(15)$] which deploy along the two crystallographic axes a and b (**Figure 2b** and **c**) [8].

4. Luminescent properties

Photoluminescence spectra were measured using a Cary Eclipse (Agilent Technologies) fluorescence spectrophotometer in a quartz cell (1.1 cm cross section) equipped with a xenon lamp and a dual monochromator. The measurements in solvents of different polarities were carried out at ambient temperature (298 K) with the slit ex/em = 20/10 nm. The photoluminescence properties of $\{(C_{12}N_2H_8) \cdot H_2O\}$ in any solution were investigated in the visible region. The emission spectra of phh (10^{-4} M) in non-polar solvents, viz. benzene and toluene, show maximum at ~420 nm at λ_{ex} = 320 nm (**Figure 3**). Studies at higher concentrations of the probe were not possible as it is marginally soluble in non-polar solvents. In polar solvents, viz. methanol, ethanol and acetonitrile, the solution exhibit emission maximum at

D—H⋯A	D—H	H⋯A	D⋯A	D—H⋯A
O1W—H1W⋯O1Wi	0.8 (5)	2.2 (4)	2.95 (4)	163.00
O2W—H2W⋯N1A	0.9(3)	2.1 (2)	2.92 (4)	152.00
O2W—H2W⋯N2A	0.9(3)	2.5 (2)	3.18 (4)	135.00
O3W—H3W⋯O3Wii	0.84(19)	2.1 (2)	2.96 (4)	174.00
O1W—H11W⋯N1B	1.10(19)	1.9 (2)	2.90 (3)	152.00
O1W—H11W⋯N2B	1.10(19)	2.4 (3)	3.18 (3)	125.00
O2W—H22W⋯O2Wiii	0.8(2)	2.1 (2)	2.94 (3)	169.00
O3W—H33W⋯N1C	0.86(18)	2.5 (2)	3.16 (3)	138.00
O3W—H33W⋯N2C	0.86(18)	2.2 (2)	2.97 (3)	148.00
C1B—H1B⋯O1Wi	0.9300	2.5900	3.44 (5)	152.00
C3A—H3A⋯N1Civ	0.9300	2.4900	3.28 (5)	142.00
C8C—H037⋯N2Bv	0.9200	2.4700	3.31 (5)	151.00
C5B—H5B⋯N2A	0.9300	2.5700	3.41 (5)	151.00
C8B—H8B⋯N2Avi	0.9300	2.5000	3.25 (5)	139.00

Symmetry codes: (i) −y + 1, x − y + 1, z + 1/3; (ii) −x + y + 1, −x + 1, z − 1/3; (iii) −y, x − y, z + 1/3; (iv) −x + y + 1, −x + 1, z + 2/3; (v) −x + y, −x, z − 1/3; (vi) −y, x − y, z − 2/3.

Table 1.
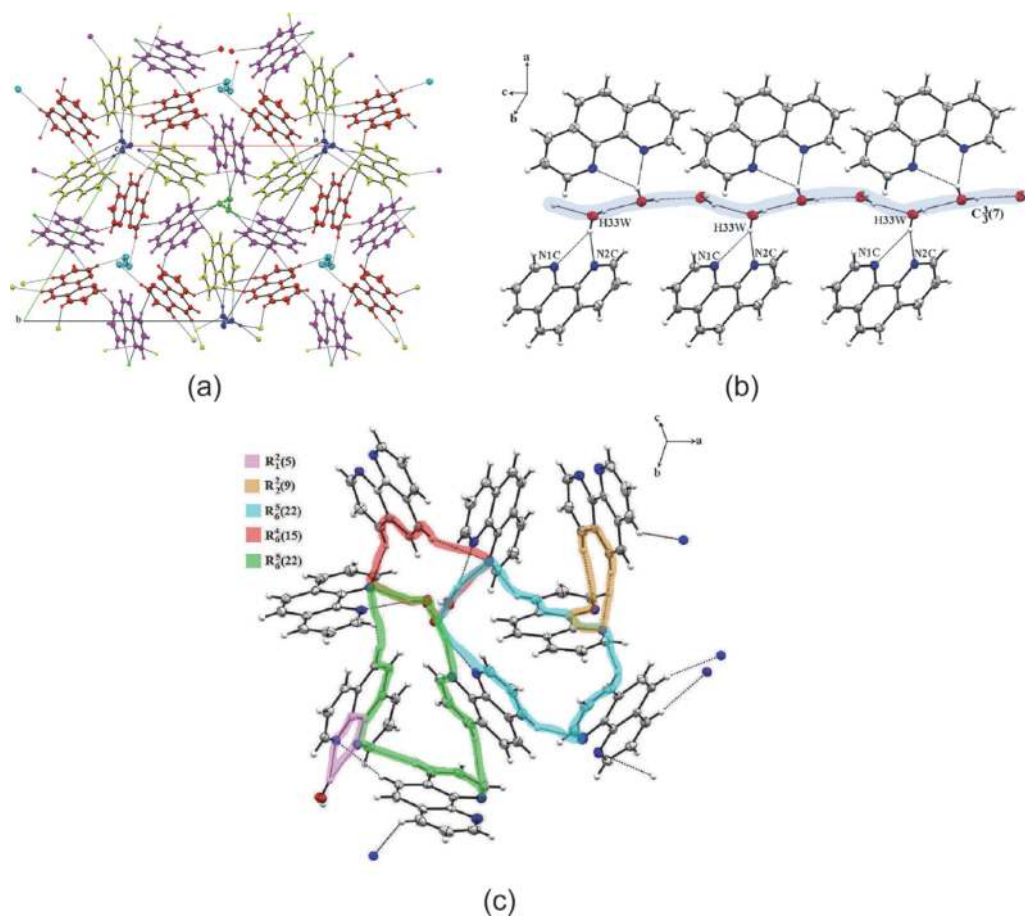*Hydrogen bond geometry (Å, °).*

Figure 2.
(a) Partial view of the packing in the phh, showing the O—H O, O—H N, C—H O and C—H N hydrogen bonds. (b) Partial view of the packing in the phh, showing the formation of the infinite chain $C^3_3(7)$. (c) Graph set $R^2_1(5)$, $R^2_2(9)$, $R^5_6(22)$ and $R^4_6(15)$ motifs. Atoms are represented as circles of different radii. Hydrogen bonds are shown as dashed lines.
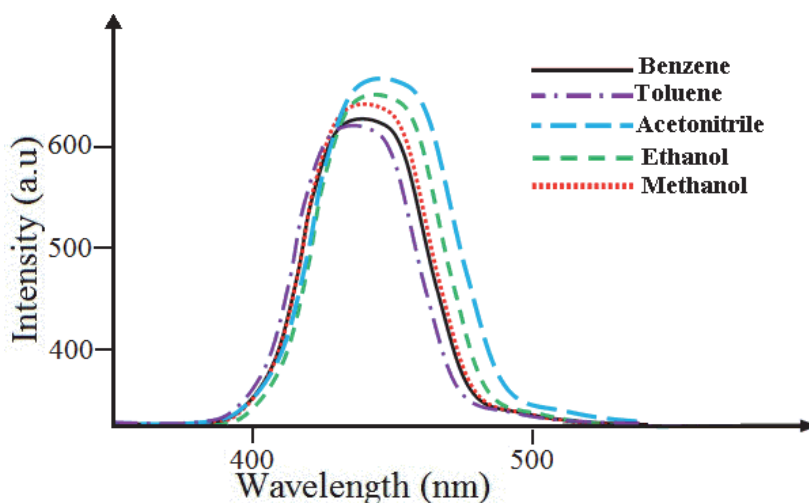

Figure 3.
Fluorescence spectra of phh in polar and non-polar solvent.

~440 nm, which resembles with the emission spectrum in non-polar solvents. This also indicates the absence of any aggregates or other conformers in the ground state. The studied compound was found to be fluorescently active in solution at room

temperature showing an intense blue fluorescence with high fluorescent quantum yield, independent of the excitation wavelength in different solvents. The spectra clearly reveal that the emission originate from an excited state-charge transfer state π-π^* because of the presence of N atoms. Thus, the compound phh may be a candidate for blue-light luminescent materials.

5. Theoretical analysis

All geometry optimizations of the molecular structure of phh were performed within the Amsterdam Density Functional (ADF) software [9], and all of theoretical calculations were carried out by the density functional theory (DFT), using the Perdew, Burke and Ernzerhof's exchange functional along with generalized gradient approximations, exchange and correlation functional GGA (PBE) [10, 11], employing the triple-zeta polarized (TZP) basis set.

Singlet excited states were optimized using time-dependent DFT (TD-DFT) calculations [12–15].

The geometric optimization has been carried on the molecular structure of phh. The ground state geometry was adapted from the X-ray data. Calculated structural parameters reveal a good agreement with the original X-ray diffraction data, which indicates significant stability of both compounds (**Table 2**).

5.1 TD-DFT absorption spectra

The time-dependent density functional theory calculations were performed on this compound, with the aim to identify the nature of the electronic transitions.

N1A—C1A	1.32 (4)	N2B—C10B	1.34 (5)
N1A—C12A	1.36 (4)	N2B—C11B	1.36 (4)
N2A—C10A	1.32 (4)	N1C—C12C	1.35 (4)
N2A—C11A	1.36 (4)	N1C—C1C	1.33 (4)
N1B—C12B	1.36 (4)	N2C—C11C	1.36 (4)
N1B—C1B	1.32 (5)	N2C—C10C	1.33 (4)
C1A—N1A—C12A	117 (3)	N1B—C1B—C2B	124 (3)
C10A—N2A—C11A	117 (3)	N2B—C10B—C9B	123 (3)
C1B—N1B—C12B	119 (3)	N2B—C11B—C7B	123 (3)
C10B—N2B—C11B	117 (3)	N2B—C11B—C12B	118 (2)
C1C—N1C—C12C	117 (2)	N1B—C12B—C11B	119 (3)
C10C—N2C—C11C	117 (3)	N1B—C12B—C4B	122 (3)
N1A—C1A—C2A	124 (3)	N1C—C1C—C2C	124 (3)
N2A—C10A—C9A	125 (4)	N2C—C10C—C9C	125 (3)
N2A—C11A—C7A	123 (3)	N2C—C11C—C7C	123 (3)
N2A—C11A—C12A	118 (3)	N2C—C11C—C12C	118 (2)
N1A—C12A—C4A	123 (3)	N1C—C12C—C4C	124 (3)
N1A—C12A—C11A	118 (3)	N1C—C12C—C11C	118 (2)

Table 2.
Selected geometric parameters (Å,°).

The absorption spectra of the studied compound are shown in **Figure 1**. The computed absorption bands, dominant transitions, characters and oscillator strengths (f) are given in **Table 3**.

The compound phh that absorbs in the region (λ = 165–280 nm) appears in **Figure 4**, and it shows three peaks with maxima at λ = 190, 225 and 268. **Table 3** clearly indicates that the lowest energy and the intense peak is at λ = 268 nm (E = 4.62 eV), transition character as corresponding it results from a transition H−2 to L+1. From **Figure 4** we observe two absorption peaks positioned at λ = 225 and 190 nm; the absorption bands correspond to the H−1 to L+3 and H−3 to L+2, respectively; and these transitions are affected to a π-π^* transition.

5.2 AIM topological analysis

Bader and Essen have shown that that the negative value of $\nabla^2(\rho)$ indicates that there is an electronic charge concentration at the BCP, which implies that the nature of the bond is covalent. For intermolecular interactions, is less weak and $\nabla > 0$, which implies the presence of a hydrogen-bonding interaction [16, 17].

The atoms in molecules (AIM) theory for part B (C1B to C12B/O1W) was applied to analyze the electron densities and their properties; details obtained from this approach are shown in **Table 4**. **Figure 5** shows the existence of a bond critical point between all of each two bonded atoms in part B.

We notice from **Table 4**, the values $\rho > 0.2$ and $\Delta < 0$ indicate that covalent bonds are present. And for the bond between N1B and H11W, we notice that $\rho = 0.034$ is very weak and $\Delta = 0.091 > 0$ (see **Table 4**) which indicate the presence of a strong hydrogen-bonding interaction. These results are in good agreement with those obtained by experimental refinement.

λ (nm)	f	E (ev)	Transition	Character
268	0.48	4.62	H−2 to L+1	π-π^*
225	0.47	5.49	H−1 to L+3	π-π^*
190	0.20	6.49	H−3 to L+2	π-π^*

Table 3.
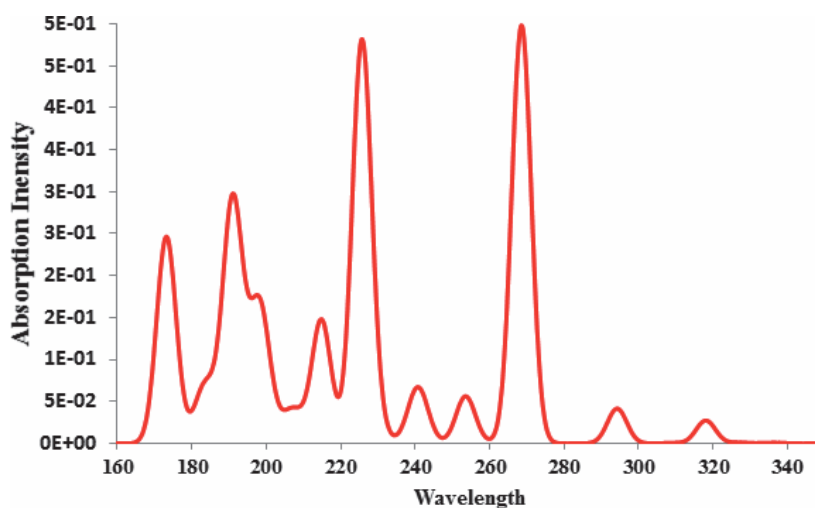*The calculated optical transition energies and their corresponding oscillator strengths (f) for phh.*

Figure 4.
TD-DFT absorption spectra of phh.

Basins	ρ	∇	$|V|/G$	H
N1B—H11W	0.034	0.091	1.063	−0.001
N1B—C1B	0.329	−0.869	3.275	−0.387
N1B—C12B	0.341	−0.946	3.138	−0.444
O1W—H1W	0.346	−1.686	6.984	−0.506
O1W—H11W	0.327	−1.685	7.426	−0.499

Table 4.
Results of atoms in molecule approach for part B of phh molecule.
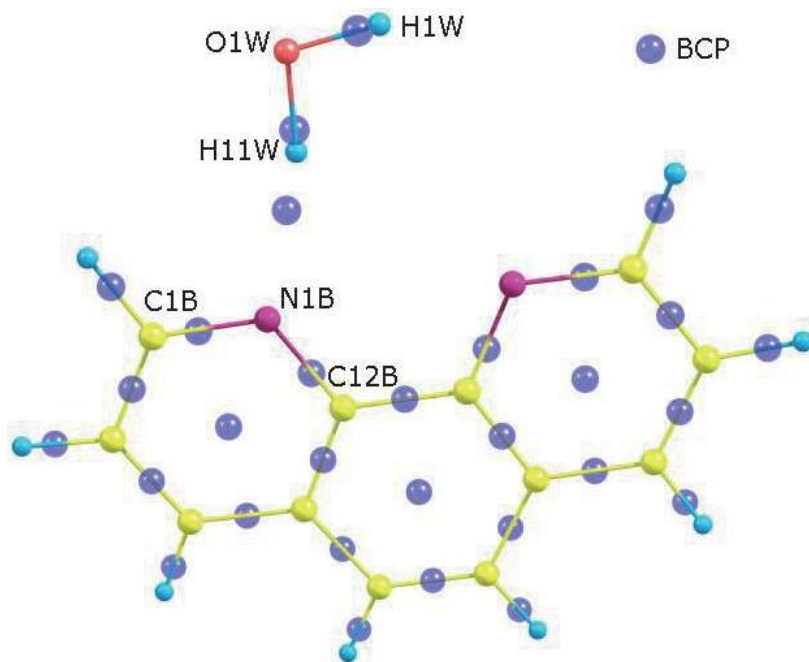
Figure 5.
The critical point founded between every pair of atoms in part B.

5.3 Orbital analysis and molecular electrostatic potential

The energy diagram of the molecular orbitals obtained by DFT approach for part B of compound phh is shown in **Figure 6**.

The HOMO and LUMO are important orbitals in a molecule; the gap between the occupied and vacant orbitals (HOMO/LUMO) is remarkable in the compound (2.92 eV; see **Figure 6**) and predicts its stability.

The highest occupied molecular orbital (HOMO) is mainly delocalized on the oxygen atom (93%), while it is found that the carbons of the cycles contribute strongly in the composition of the LUMO orbital with a participation rate of 88%.

The molecular electrostatic potential is a very important element for the illustration and visualization of the charge region variability and allows identifying the electrophilic and nucleophilic attack sites as well as the hydrogen-bonding interactions [18–21].

The blue region represents positive MESP, and the red region represents negative ESP, while the green region refers to the neutral region. From the MESP surface diagram, it can be seen that negative regions (red) are mainly localized over the oxygen and the nitrogen atom, while the positive regions (blue) are distributed over
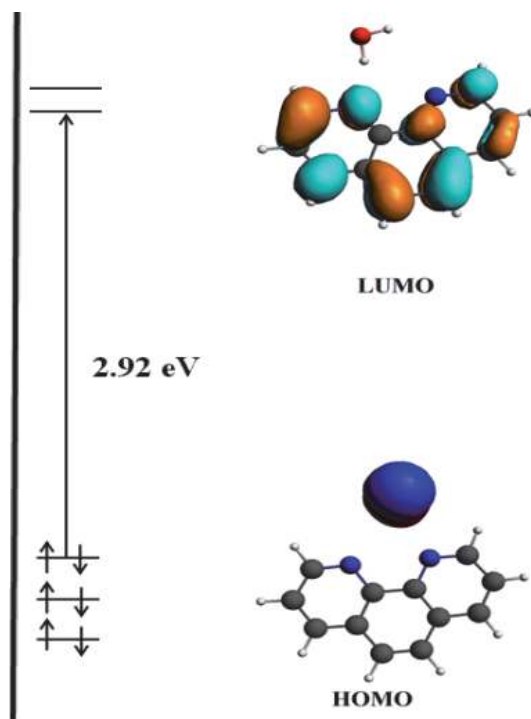
Figure 6.
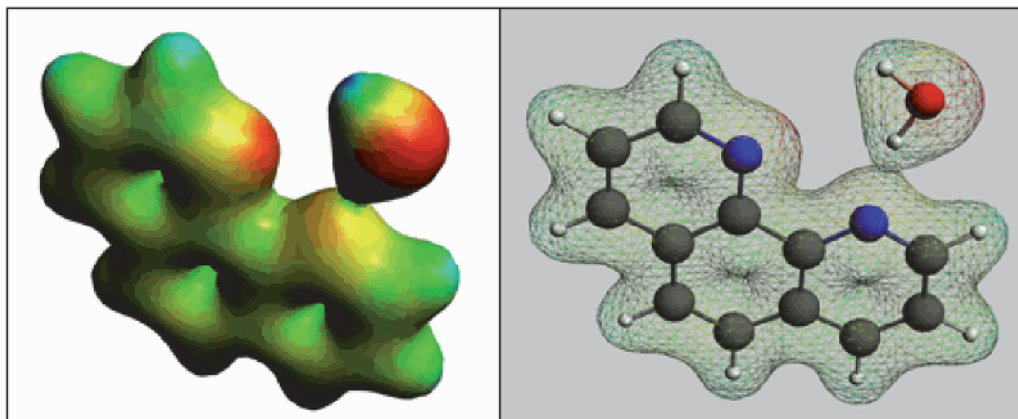*Frontier molecular orbital diagram of part B.*

Figure 7.
MEP surface diagram of part B.

the H atoms. **Figure 7** shows the presence of a hydrogen-bonding interaction between N1B and H11W.

6. Crystallization

On a Perkin-Elmer spectrometer, infrared spectra were recorded at room temperature in an interval of 500–4000 cm^{-1}.

The compound was crystallized by dissolving the 1–10 phenanthroline hydrate (1 g) in mixture solution of ethanol-water (V/V = 1:1). The solution was preserved at room temperature under agitation during 4 h. After a slow evaporation in the interior of 2 days, transparent prism crystals were obtained.

The crystals formed were washed and filtered using 20 ml of water.

The most important infrared wavelength (cm^{-1}):

(1): 3400 (vs), 3084 (m), 1632 (w), 1617 (w), 1575 (s), 1564 (m), 1502 (s), 1443 (w), 1414 (vs), 1340 (w), 1285 (vw), 1208 (w), 1132 (m), 1082 (w), 1031 (w), 987 (m), 860 (vw), 764 (w), 733 (vs).

7. Programmes

Computer programmes by Bruker *APEX2* (2006) [22]; *SAINT* (Bruker, 2006) [22]; *SAINT*, *SIR2002* [23], and *SHELXL2008* [24]; *WinGX* [25]; *Mercury* Version 1.4 [26]

8. Refinement

Crystal data, data collection and structure refinement details are summarized in **Table 5**. H atoms were placed at calculated positions with C⎯H = 0.93 Å (aromatic

	(hpp)
	Crystal data
Chemical formula	C13.50H11.25N2.25O1.13
Mr	223.00
Crystal system, space group	Trigonal, P31
Temperature (K)	293
a, c (Å)	17.5075 (7), 8.4300 (4)
V ($Å^3$)	2237.72 (14)
Z	8
Radiation type	Mo Kα
μ (mm^{-1})	0.09
Crystal size (mm)	$0.2 \times 0.1 \times 0.08$
	Data collection
Diffractometer	Bruker APEX-II CCD
Absorption correction	—
No. of measured, independent and observed [I > 2σ(I)] reflections	13,243, 5115, 4195
Rint	0.046
$(\sin θ/λ)$max ($Å^{-1}$)	0.596
	Refinement
R[F2 > 2σ(F2)], wR(F2), S	0.047, 0.098, 1.06
No. of reflections	5115
No. of parameters	418
No. of restraints	10
Δρmax, Δρmin (e $Å^{-3}$)	0.25, −0.19
Absolute structure	[27]
Absolute structure parameter	0.4 (15)

Table 5.
Experimental details.

H atoms) and refined in riding mode with $U_{iso}(H) = 1.2U_{eq}(C)$. The O-bound H atoms were located in a Fourier map and refined with O—H restraint of 0.85 (1)Å ($U_{iso}(H) = 1.5U_{eq}(O)$).

9. Conclusion

The experimental and theoretical charge-density analysis has been performed to understand the topological and electrostatic properties of the 1–10 phenanthroline hydrate molecule. The crystal structure reveals the molecule forming O—H⋯O, O—H⋯N, C—H⋯O and C—H⋯N types of interactions with the neighboring molecules. Furthermore, photoluminescence studies indicate that the hpp is fluorescently active in solution at room temperature and reveal that the emission originate from an excited state-charge transfer state π-π* which is proven by TD-DFT analysis.

The AIM analysis shows the existence of a bond critical point (BCP) between N1B and H11W. We notice that ρ = 0.034 is very weak and Δ = 0.091 > 0 which confirms that this interaction is the strongest interaction in the molecule (hydrogen-bonding interaction). These results are in good agreement with those obtained by experimental refinement.

The structural, topological and electrostatic properties of the 1–10 phenanthroline hydrate molecule obtained from the X-ray diffraction method may be useful to design a new candidate of blue-light luminescent materials.

Acknowledgements

Author details

Ouahida Zeghouan[1]* , Seifeddine Sellami[2] and Mohamed AbdEsselem Dems[1]

1 Biotechnology Research Center (CRBt), Constantine, Algeria

2 Laboratoire Pollution et Traitement des Eaux, Département de Chimie, Faculté des Sciences Exactes, Université Frères Mentouri Constantine 1, Constantine, Algeria

*Address all correspondence to: ouahida.zeghouan@gmail.com

IntechOpen

References

[1] Sastri CV, Eswaramoorthy D, Giribabu L, Maiya BG. DNA interactions of new mixed-ligand complexes of cobalt(III) and nickel(II) that incorporate modified phenanthroline ligands. Journal of Inorganic Biochemistry. 2003;**94**: 138-145

[2] Cohen G, Eisenberg H. Viscosity and sedimentation study of sonicated DNA–proflavine complexes. Biopolymers. 1969;**8**:45-55

[3] Satyanarayana S, Dabrowiak JC, Chaires JB. Neither DELTA- nor LAMBDA-tris(phenanthroline) ruthenium (II) binds to DNA by classical intercalation. Biochemistry. 1992;**31**:9319-9324

[4] Bader RFW. Atoms in Molecules: A Quantum Theory. Oxford, New York: Clarendon Press; 1995

[5] Coppens P. X-Ray Charge Density and Chemical Bonding. Oxford University Press; 1997

[6] Gropper H, Doerrr F. Berichte der Bunsengesellschaft für physikalische Chemie. 1963;**67**:46-54

[7] Shulman SG. The IR spectrum of 4,7-phenanthroline in the region 650-900 cm-1 has been analyzed, and the C—H ... 77. Fluorescence News. 1973;**7**:33

[8] Bernstein J, Davis RE, Shimoni L, Chang N-L. Patterns in Hydrogen Bonding Functionality and Graph Set Analysis in Crystals. Angewandte Chemie (International Ed. in English). 1995;**34**:1555-1573

[9] Baerends EJ, Ellis DE, Ros P. Self-consistent molecular Hartree—Fock—Slater calculations I. The computational procedure. The Journal of Chemical Physics. 1973;**2**(1):41-51

[10] Perdew JP, Burke K, Ernzerhof M. Generalized gradient approximation made simple. Physical Review Letters. 1997;**78**:1396-1396

[11] Langreth DC, Vosko SH. In density functional theory of many-fermion systems. Advances in Quantum Chemistry. 1990;**21**:175-175

[12] Bauernschmitt R, Ahlrichs R. Stability analysis for solutions of the closed shell Kohn–Sham equation. The Journal of Chemical Physics. 1996;**104**: 9047-9052

[13] Gross EUK, Dobson JF, Petersilka M. Density functional theory of time dependent phenomena. In: Hafner K, Houk KN, Lehn IJM, Raymond KN, Rees CW, Thiem J, Vogtle F, editors. Topics in Current Chemistry—Density Functional Theory II. Berlin: Springer; 1996. pp. 81-172

[14] Casida ME. In: Chong PD, editor. Recent Advances in Density Functional Methods. Vol. 1. Canada: University of British Columbia; 1995. pp. 155-193. ISBN: 978-981-283-058-6

[15] Gross EKU, Kohn W. Time-dependent density-functional theory. Advances in Quantum Chemistry. 1990; **21**:255-291

[16] Bader RFW, Essén H. The characterization of atomic interactions. Journal of Chemical Physics. 1984;**80**: 1943

[17] Bader RFW, Matta CF. Bonding to titanium. Inorganic Chemistry. 2001;**40**: 5603

[18] Politzer P, Daiker KC. Models for chemical reactivity. In: Deb BM, editor. The Force Concept in Chemistry. New York: Van Nostrand Reinhold; 1981. pp. 294-387

[19] Politzer P, Laurence PR, Jayasuriya K, McKinney J. Molecular

electrostatic potentials: An effective tool for the elucidation of biochemical phenomena. In: McKinney J, editor. Structure Activity Correlation in Mechanism Studies and Predictive Toxicology, Environ. 1985;**61**:191-202

[20] Politzer P, Murray JS. Theoretical Biochemistry and Molecular Biophysics: A Comprehensive Survey. Vol. 2. Schenectady, NY: Adenine Press; 1991. pp. 165-191

[21] Scrocco E, Tomasi J. Topics in Current Chemistry. Vol. 42. Berlin: Springer-Verlag; 1973. p. 95

[22] Bruker. APEX2 and SAINT. Madison,Wisconsin, USA: Bruker AXS Inc.; 2006

[23] Burla MC, Camalli M, Carrozzini B, Cascarano GL, Giacovazzo C, Polidori G, et al. SIR prorram. Journal of Applied Crystallography. 2003;**36**:1103

[24] Sheldrick GM. Crystal structure refinement with SHELXL. Acta Crystallographica. 2008;**A64**:112-122

[25] Farrugia LJ. WinGX and ORTEP for Windows: An update. Journal of Applied Crystallography. 2012;**45**:849-854

[26] Macrae CF, Bruno IJ, Chisholm JA, Edgington PR, McCabe P, Pidcock E, et al. New features for the visualization and investigation of crystal structures. Journal of Applied Crystallography. 2008;**41**:466-470

[27] Flack HD. On enantiomorph-polarity estimation. Acta Crystallographica. 1983;**A39**:876-881